The Chott El Djerid, Tunisia: Observation and Discussion of a SAR Phase Signature Over Evaporitic Soils

Philippe Paillou, Sarah Sufyar, and Anthony Freeman

***Abstract*—The presence of water in arid regions is correlated to large evaporitic deposits, with high concentration of salts. Polarimetric synthetic aperture radar (SAR) observations over such areas show high variations for both the amplitude and phase of the backscattered copolarized signal. This is due to a large dynamic range for both surface roughness and dielectric constant parameters, between the wet and dry seasons: crystallized salt is rough and presents a low dielectric constant, whereas saline water corresponds to smooth and conductive surfaces. We observed a complete seasonal cycle over the chott El Djerid playa, in southern Tunisia, using the 5.6-GHz C-band polarimetric SAR on-board RADARSAT-2. One SAR image acquisition was performed every 24 days, from February to September 2009. In addition to expected variations in the radar backscattered power, we observed significant changes in the phase difference between horizontally and vertically polarized channels. In order to explain such a phase effect, we first considered the arguments of the Fresnel reflectivity coefficient when approaching the Brewster angle, for materials presenting a high loss tangent. A more complete analytical modeling derived from the integral equation model approach confirmed this hypothesis.**

***Index Terms*—Chott, El Djerid, integral equation model (IEM), phase, playa, polarimetry, synthetic aperture radar (SAR), Tunisia.**

I. Introduction

SALT accumulation occurs in arid regions where evaporation exceeds water supply. The later can be natural (rainfall, groundwater) or artificial (irrigation). The quality of agricultural soils can then be degraded by the increase of salt concentration over surfaces, while natural salt deposits in arid regions, which are named playas, can be used as surface clues of groundwater presence. More than 15 years ago, radar remote sensing was shown to be sensitive to soil salinity, since the complex dielectric constant of salt plays an important role in the radar backscatter [21], [23]. In addition to their dielectric constant, playas also present a strong variation of their surface roughness with time, ranging from perfectly smooth when flooded by water to rough when dry and covered by a salt crust. Both the dielectric constant and the roughness state of such surfaces highly impact the amplitude of the backscattered power in radar remote sensing [24].

Wadge *et al.* [25] were the first to monitor changes over evaporitic surfaces using synthetic aperture radar (SAR) images provided by the ERS-1 satellite. They observed that the radar backscatter increased during the dry season over the chott El Djerid playa, in southern Tunisia, as its surface is more and more covered by halite crystals. They later derived an empirical relationship between the radar backscatter coefficient and the surface roughness, in order to estimate the rate of water evaporation [1], [26]. In parallel, several laboratory experiments were conducted using soil–water–salt mixtures, in order to study the dependence of the complex dielectric constant with respect to the water and salt concentrations [14], [20]. It was shown that the soil moisture affects the real part of the dielectric constant, whereas the presence of salt dramatically increases the imaginary part of the dielectric constant. A very complete study of the radar signature of saline deposits was conducted over the Death Valley, CA, USA, by Lasne *et al.* [15]. Field measurements of the dielectric properties of various salt deposits and saline water were realized over the salt pan of Cottonball Basin, and they were used as input parameters to model the radar response at both C- and L-bands. Analytical simulations of the copolarized amplitude ratio and phase difference were proposed and compared to actual airborne and spaceborne SAR data acquired by the Airborne Synthetic Aperture Radar (operated by Jet Propulsion Laboratory) (AIRSAR) and Spaceborne Imaging Radar C (onboard Space Shuttle in 1994) (SIR-C) sensors. It was shown in particular that the phase difference between horizontally and vertically polarized SAR acquisitions is a promising polarimetric signature to detect and monitor salt deposits.

Using time series of C-band polarimetric acquisitions by the RADARSAT-2 satellite, we monitored a complete wet-to-dry cycle of the playa deposit of the chott El Djerid in Tunisia and observed the temporal evolution of the copolarized phase difference. While Lasne *et al.* [15] proposed a complex two-layer model to explain the observed copolarized phase difference, we propose here a more simple explanation to the copolarized phase behavior, which is based on the Fresnel reflectivity coefficients when approaching the Brewster angle, for materials

Manuscript received March 25, 2013; revised July 15, 2013 and October 3, 2013; accepted November 4, 2013. Date of publication December 20, 2013; date of current version May 1, 2014. This work was supported in part by the French Space Agency (CNES) and in part by the Programme National de Télédétection Spatiale (INSU).

P. Paillou is with the University of Bordeaux, Unité Mixte de Recherche (UMR) 5804 Laboratoire d'Astrophysique de Bordeaux (LAB), 33270 Floirac, France (e-mail: paillou@obs.u-bordeaux1.fr).

S. Sufyar is with the University of Bordeaux, UMR 5804 (LAB), 33270 Floirac, France, and also with the Laboratoire de l'Intégration du Matériau au Système (IMS), 33607 Pessac, France.

A. Freeman is with the Jet Propulsion Laboratory, California Institute of Technology, Pasadena, CA 91109 USA.

Color versions of one or more of the figures in this paper are available online at http://ieeexplore.ieee.org.

Digital Object Identifier 10.1109/TGRS.2013.2292822

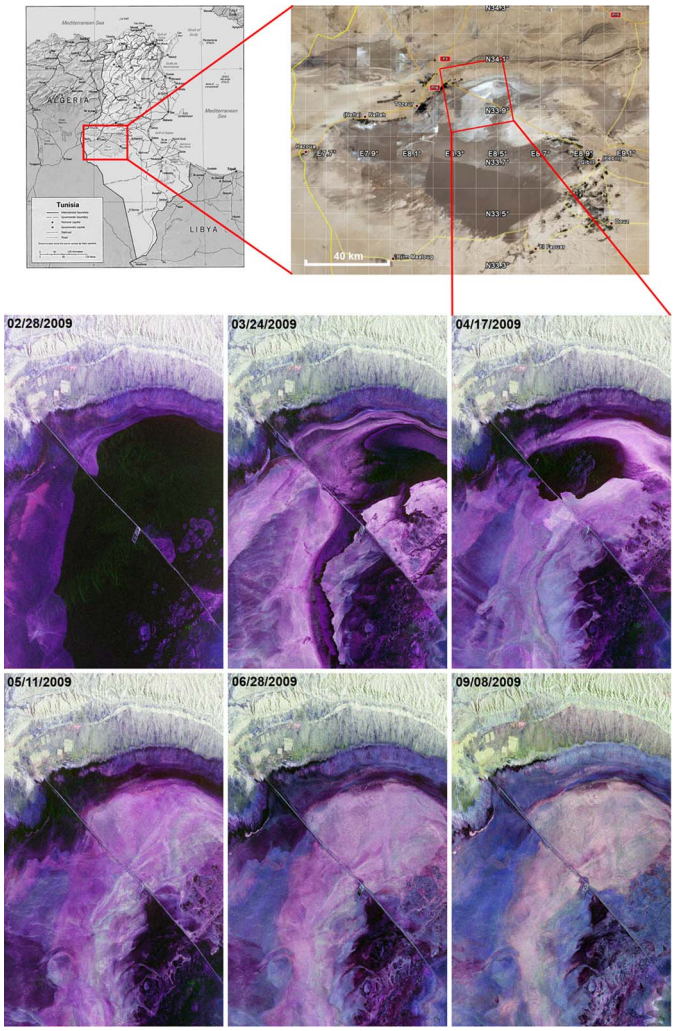

Fig. 1. Chott El Djerid, central Tunisia, imaged by the RADARSAT-2 SAR, from February to September 2009. SAR scenes are presented using the Pauli decomposition color-coding scheme (red = HH − VV; green = HV; blue = HH + VV).

presenting a high loss tangent. A more developed analytical approach, which is based on the integral equation model (IEM) proposed by Fung *et al.* [9], confirms our hypothesis.

II. Chott El Djerid, Tunisia

The Chotts Trough region in southern Tunisia is part of a foreland basin associated with the Atlas fold and thrust belt [22]. The chott El Djerid is the largest of three modern terrestrial playas in southern Tunisia. It occupies a synclinal basin and covers an area of 110 km × 70 km between the Tozeur and Kebili oasis (see Fig. 1). It is a flat area, with a mean altitude of 15 m, centered at 33.73° N−8.40° E. The chott El Djerid forms the northeastern extremity of the Bas Sahara artesian basin. Aquifers emerge at the surface of the Chotts Trough region, through a thin clay layer of the Quaternary age [18], allowing temporary flooding of the playa depressions in winter. The mean annual rainfall for the area is around 100 mm, while evaporation has a mean annual value of 1500 mm. The negative annual balance leads to high evaporation rates and sedimentation of salts, by evaporation of groundwater.

Fig. 2. Pictures of the chott El Djerid taken during November 2008. (Upper left) Road crossing the chott between Tozeur and Kebili, with the chott being partially inundated. (Upper right) Salt and gypsum (desert roses) exposed along the road. (Lower left) Salty mud with halite salt crust forming by evaporation of saline water. (Lower right) Precipitation of halite crystals on the border of a small saline pond.

The chott El Djerid goes through four main flooding stages from winter to summer [3]. The first stage is the flooding of the chott (December–February), when both groundwater and rainfall fill in the depression, creating a shallow lake and rapidly dissolving the pre-existing salt pan. The second stage (May–June) involves evaporative concentration of the shallow lake, with precipitation of gypsum and halite at its edges. The third stage (July–September) represents the final evaporation of ponded water, with formation of large halite salt crust. The final stage (October–November) involves the total dessication of the chott and the precipitation of most soluble salts, leaving a large central saline pan dominated by halite. This process, together with intensive irrigation in the chott region, leads to an increasing salinization of the groundwater [11]. Fig. 2 shows the various surface states and salt deposits observed on the chott El Djerid during November 2008.

The high temporal dynamics of the chott El Djerid was monitored using time series of remotely sensed images: optical and near-infrared data provided by the Advanced Very High Resolution Radiometer sensor [4], [5] allowed to map the inundation phases related to groundwater infiltration and rainfall events, while microwave data provided by the ERS-1 SAR [25], [26] allowed to monitor the evaporation and salt pan formation process. More recently, Frison *et al.* [8] have studied the temporal variations of the chott El Djerid over several years, using various C-band active sensors (Advanced SCATterrometer (onboard METOP-A satellite), Advanced Synthetic Aperture Radar (onboard ENVISAT satellite), and RADARSAT-2). We shall in the following consider time series of full-polarimetric C-band SAR acquisitions by RADARSAT-2 over the central part of the chott El Djerid, in order to monitor the temporal behavior of the copolarized phase difference.

III. Observation of a Copolarized SAR Phase Difference

We dispose of temporal series of RADARSAT-2 full-polarimetric SAR scenes, which were acquired over the chott

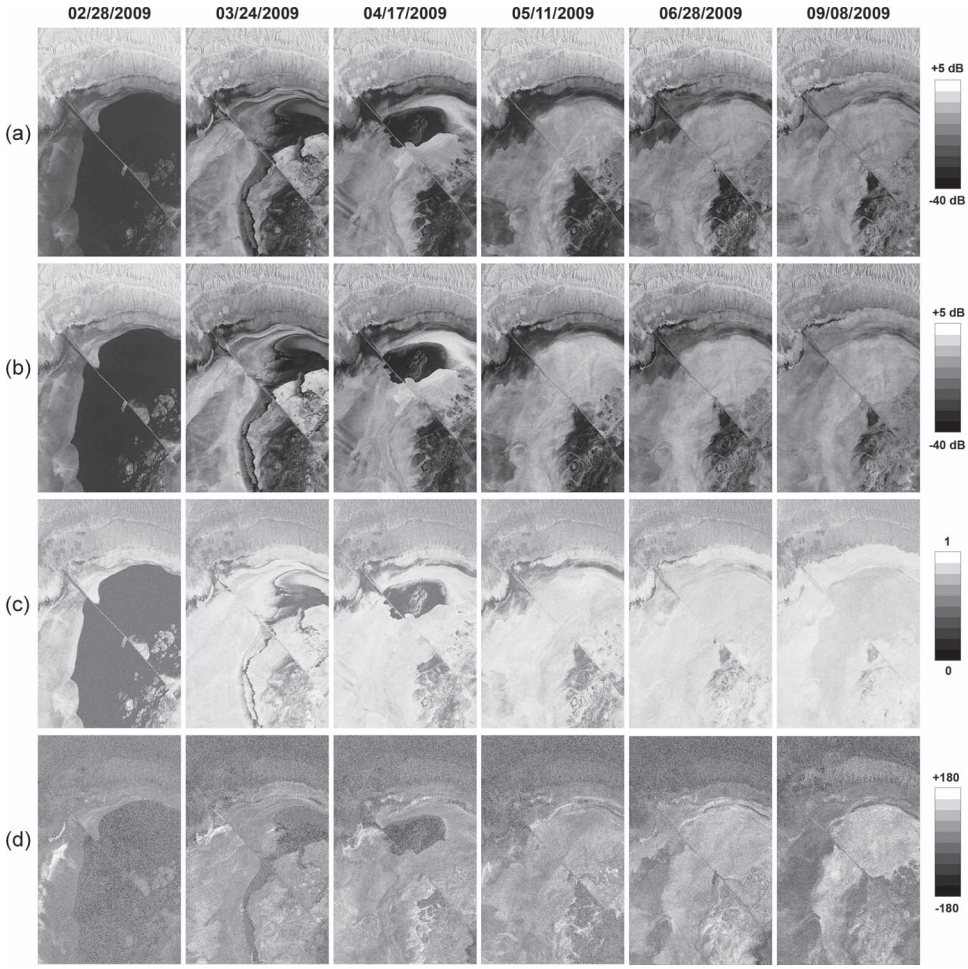

Fig. 3. Evolution of the copolarized backscattered power (a) σ^0_{HH} and (b) σ^0_{VV}, (c) the HH–VV coherence γ_{HHVV}, and (d) the copolarized phase difference Φ_{HHVV}, over the chott El Djerid from February to September 2009.

El Djerid from February to September 2009. Ten scenes were acquired at an interval of 24 days, with the same incidence angle of 38.5° using the Fine Quad-Pol beam mode (FQ19), at a resolution of 5.4 m in range and 8.0 m in azimuth, with a 25 km × 25 km coverage [17]. The period of acquisitions, i.e., from winter to summer, allowed us to observe the evaporation process over the chott, where surface evolves from completely flooded to dry. With regard to the total radar backscattered power, the signal ranges from very low (−34 dB) for smooth flooded surfaces to rather high (−11 dB) for dry and rough salt deposits (see Fig. 1).

We obtained the RADARSAT-2 scenes in a single-look complex mode, i.e., each pixel contains the 2 × 2 complex scattering matrix S, which relates the incident wave E^i to the scattered wave E^s [16], as follows:

$$E^s = \frac{e^{-jkr}}{r} S E^i = \frac{e^{-jkr}}{r} \begin{bmatrix} S_{\mathrm{hh}} S_{\mathrm{hv}} \\ S_{\mathrm{vh}} S_{\mathrm{vv}} \end{bmatrix} E^i \quad \sigma_{\mathrm{pp}} = 4\pi |S_{\mathrm{pp}}|^2 \qquad (1)$$

where S_{qp} are the complex scattering coefficients, r is the distance between the radar and the surface, k is the wavenumber, and the term (e^{-jkr}/r) takes into account the free-space propagation effects in both amplitude and phase. The radar cross section σ_{pp} is related to the scattering matrix, as indicated in (1). The PolSARpro software [http://earth.eo.esa.int/polsarpro/] was used to extract the 3 × 3 polarimetric covariance matrix C_3 for each image (no spatial ensemble averaging) [16], as follows:

$$C_3 = \begin{bmatrix} |S_{\mathrm{hh}}|^2 & \sqrt{2} S_{\mathrm{hh}} S^*_{\mathrm{hv}} & S_{\mathrm{hh}} S^*_{\mathrm{vv}} \\ \sqrt{2} S_{\mathrm{hv}} S^*_{\mathrm{hh}} & 2|S_{\mathrm{hv}}|^2 & \sqrt{2} S_{\mathrm{hv}} S^*_{\mathrm{vv}} \\ S_{\mathrm{vv}} S^*_{\mathrm{hh}} & \sqrt{2} S_{\mathrm{vv}} S^*_{\mathrm{hv}} & |S_{\mathrm{vv}}|^2 \end{bmatrix} \qquad (2)$$

from which we easily derived the copolarized backscattered power σ^0_{HH} and σ^0_{VV}, the HH–VV coherence γ_{HHVV} (using a three-pixel window size for spatial averaging), and the copolarized phase difference Φ_{HHVV}, as follows:

$$\begin{aligned} \sigma^0_{\mathrm{HH}} &= \sqrt{C_{11}} \qquad \sigma^0_{\mathrm{VV}} = \sqrt{C_{33}} \\ \gamma_{\mathrm{HHVV}} &= \left| \frac{\langle C_{13} \rangle}{\sqrt{\langle C_{11} \rangle \langle C_{33} \rangle}} \right| \\ \Phi_{\mathrm{HHVV}} &= \arg(S_{\mathrm{hh}}) - \arg(S_{\mathrm{vv}}) = \arg(C_{13}). \end{aligned} \qquad (3)$$

The resulting images are shown in Fig. 3. Regions outside the chott (northern part of the SAR scenes) present a quite constant backscattered power, HH–VV coherence, and phase difference, while the saline surfaces inside the chott depression exhibit a strong temporal variation. In particular, the copolarized phase difference shown in Fig. 3(d) shows clear structures, which allow to discriminate between flooded (dark patches in the February, March, and April scenes) and dry (bright patches in the March, April, May, June, and September scenes) surfaces.

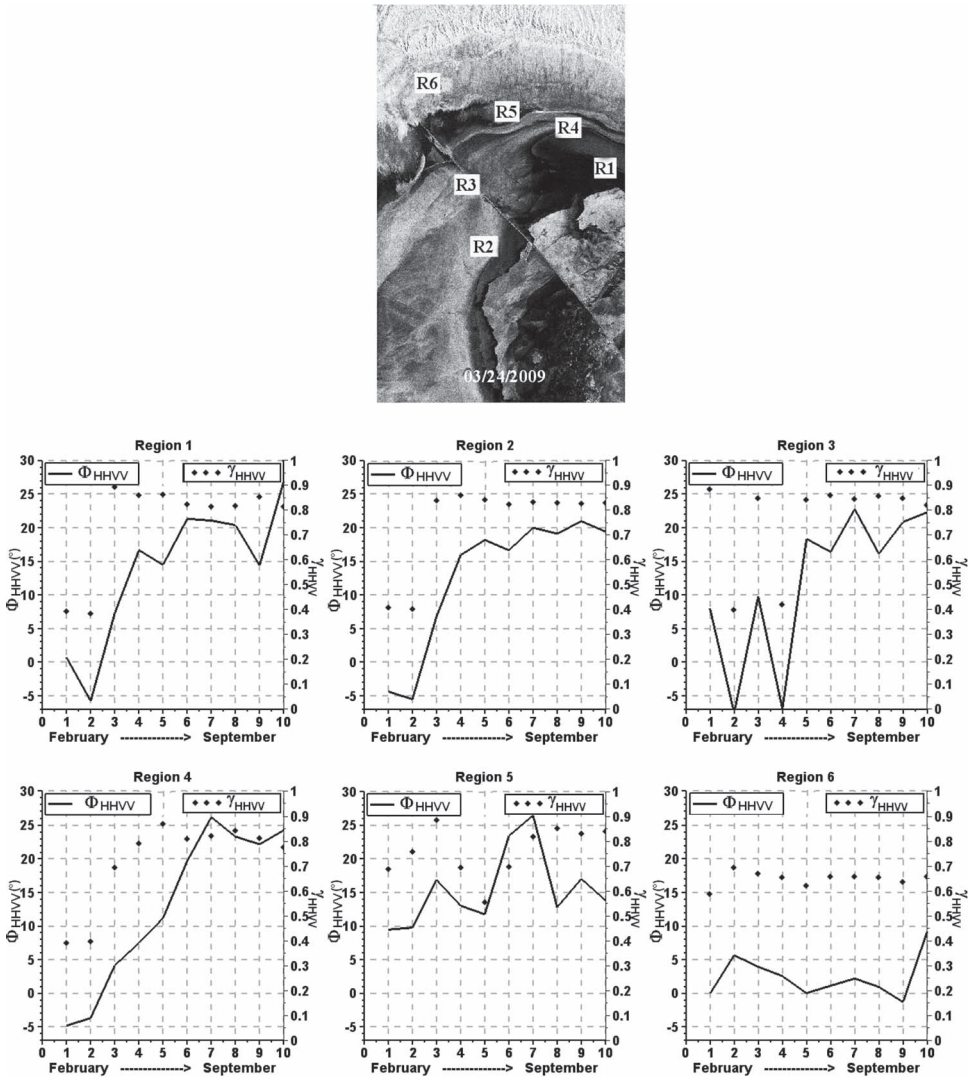

Fig. 4. (Top) Six selected regions of interest and (bottom) variation of the corresponding averaged copolarized phase difference Φ_{HHVV} (plain line) and HH–VV coherence γ_{HHVV} (dots), with respect to time.

For the flooded areas, the radar backscattered power is low, i.e., close to the noise level of the sensor, leading to a low HH–VV coherence (see Fig. 3(c), February scene) and then a random copolarized phase (see Fig. 3(d), February scene). As soon as the chott surfaces dry out, the HH–VV coherence quickly increases close to one, indicating that the copolarized phase difference is not random any more. The polarimetric parameter Φ_{HHVV} then contains coherent information related to the geophysical properties of the chott surfaces.

In order to study the temporal evolution of Φ_{HHVV} into details, we selected six regions of interest, containing around 4000 pixels each: five are located inside the chott depression and experience various moisture states between completely flooded and perfectly dry, and one corresponds to bare soils located outside the chott, acting as a blank sample for nonsaline surfaces. For each region, we computed an averaged copolarized phase difference. Fig. 4 shows the location of the six regions of interest, together with the corresponding temporal evolution of γ_{HHVV} and Φ_{HHVV} from February to September 2009. Region 6, which is located outside the chott depression in a saline-free area, always presents the same flat Gaussian-distributed copolarized phase difference [see Fig. 5(a)], with a mean value around 0° and a close-to-constant HH–VV coherence, between 0.6 and 0.7. This is what is usually expected for bare soils in radar remote sensing [16], [19]. On the opposite, regions 1–5, which are located inside the chott depression, show large variations of both copolarized phase difference and HH–VV coherence. During the wet season, from February to April, the flooded areas exhibit a random copolarized phase difference, distributed between -180° and $+180^\circ$, as shown in Fig. 5(b), i.e., very smooth and reflective liquid surfaces present a specular behavior for the radar, leading to a backscattered power close to the noise level of the sensor (the Noise Equivalent Sigma Zero for the FQ19 mode is -36 ± 3 dB). This is confirmed by the corresponding low HH–VV coherence values. When computing an averaged copolarized phase value over such flooded regions, the obtained value is close to zero. When regions inside the chott start to dry, from April to September, the copolarized phase difference distribution becomes Gaussian, not zero centered, with a standard deviation around 15°, as shown in Fig. 5(b). As the copolarized phase difference distribution becomes nonrandom, the HH–VV coherence also rapidly increases, as shown in Figs. 3 and 4. Regions 1, 2, and 4, which are progressively

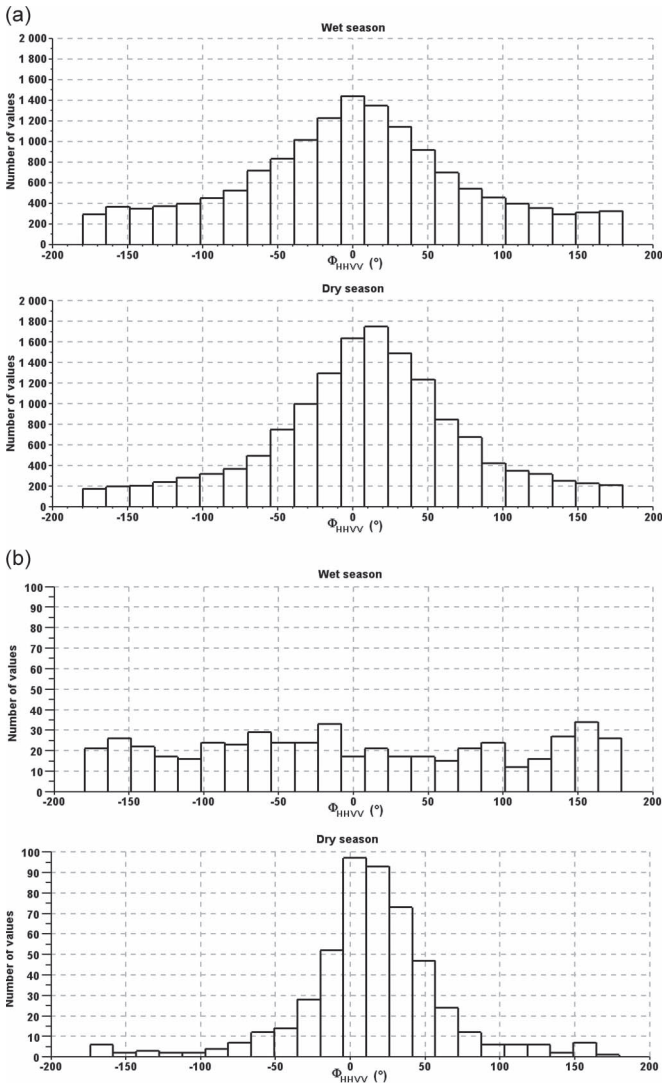

Fig. 5. (a) Copolarized phase distribution for the region of interest 6, located outside the chott depression, in (top) February and (bottom) April. (b) Copolarized phase distribution for the region of interest 1, located inside the chott depression, when (top) flooded in February and (bottom) drying in April.

and continuously drying from February to September, show an averaged copolarized phase difference that continuously increases from about 0° to values higher than 20°. Regions 3 and 5 experience alternating flooded and dry phases, with an averaged copolarized phase difference decreasing during flooding phases and increasing during drying phases. We can conclude from these observations that the averaged Φ_{HHVV} is low during humid conditions (chott flooded with saline water) and higher during dry conditions (formation of the salt crust). This is actually the opposite variation of what was observed by Lasne *et al.* [15] over the Cottonball Basin, Death Valley: they observed a decrease of the copolarized phase difference at the C-band from 11° in April 1994 (wet season) to 7° in September 1994 (dry season). We looked back to the SIR-C and AIRSAR data used and found out that only one big region of interest was considered in [15] to compute Φ_{HHVV}: this large region of interest actually mixed different types of surfaces, from liquid to very dry, and the average phase difference computed is then not representative of well-defined humidity conditions. In addition, we observed that the change in surface humidity conditions between the two acquisitions of April and September 1994 was not that obvious, i.e., the two acquisitions do not correspond to extreme cases, and deriving a trend for the variation of the copolarized phase difference is then not easy. Future investigations will be conducted to reanalyze SIR-C and AIRSAR data acquired over the Cottonball Basin and to study the influence of the radar wavelength on Φ_{HHVV}, since we dispose of C-, L-, and P-band data. Comparing curves in Figs. 4 and 6 shows that the behavior of the averaged copolarized phase difference is actually similar to the temporal evolution of the backscattered power at HH and VV polarizations: the copolarized backscattered power decreases during humid phases (the flooded surfaces are smooth and then behave as specular reflectors, with very few signal backscattered to the radar), while it increases during dry phases (the salt crust deposits are rough and then produce a more diffuse scattering of the radar wave, increasing the backscattered component). It can also be noticed in Fig. 6 that the copolarized backscattered powers for region 6, which is located outside the chott depression, remains more or less constant.

IV. Modeling of the Copolarized Phase Difference

Previous attempts to model the copolarized phase difference rely on a two-layer scattering model, i.e., the backscattered radar wave is the sum of a surface and a subsurface component [12], [13]. Although this model was proposed to explain the phase difference observed over saline surfaces [6], [7], [15], the radar penetration depth at C-band radar in saline soils is very low that all the radar wave–soil material interaction is likely to occur at the surface only. Laboratory and field measurements performed for various salt mixtures [14], [15] show that the typical dielectric constant at 5.5 GHz presents a real part ranging from 3.2 to 8.5 and an imaginary part ranging from 3.5 to 12.8. For a wavelength λ, the $1/e$ attenuation depth δ_P in a material of dielectric constant $\varepsilon = \varepsilon' - j\varepsilon''$ is given by [24]

$$\delta_P = \frac{\lambda}{4\pi}\left\{\frac{\varepsilon'}{2}\left[\sqrt{1+\left(\frac{\varepsilon''}{\varepsilon'}\right)^2}-1\right]\right\}^{-1/2}. \quad (4)$$

This yields to penetration depths at the C-band smaller than 0.5 cm in saline sediments. This is even worse for saline water: considering a typical dielectric constant $\varepsilon = 53.2 - 26.1\mathrm{j}$ [15], the penetration depth at the C-band becomes smaller than 0.25 cm.

We should then consider a pure surface scattering process to explain the observed copolarized phase difference. A simple way to start the study of the phase difference between horizontal and vertical polarizations, when dealing with the surface reflection of a planar wave, is to consider the complex Fresnel reflection coefficients. These coefficients are rather suited to the case of a bistatic radar configuration, but they can also be considered for the case of the backscattered wave in a monostatic configuration: as the backscattered radar wave remains coherent (allowing to perform the synthetic aperture process, on which SAR is based), we can make the hypothesis that the phase of the reflected and backscattered waves are at

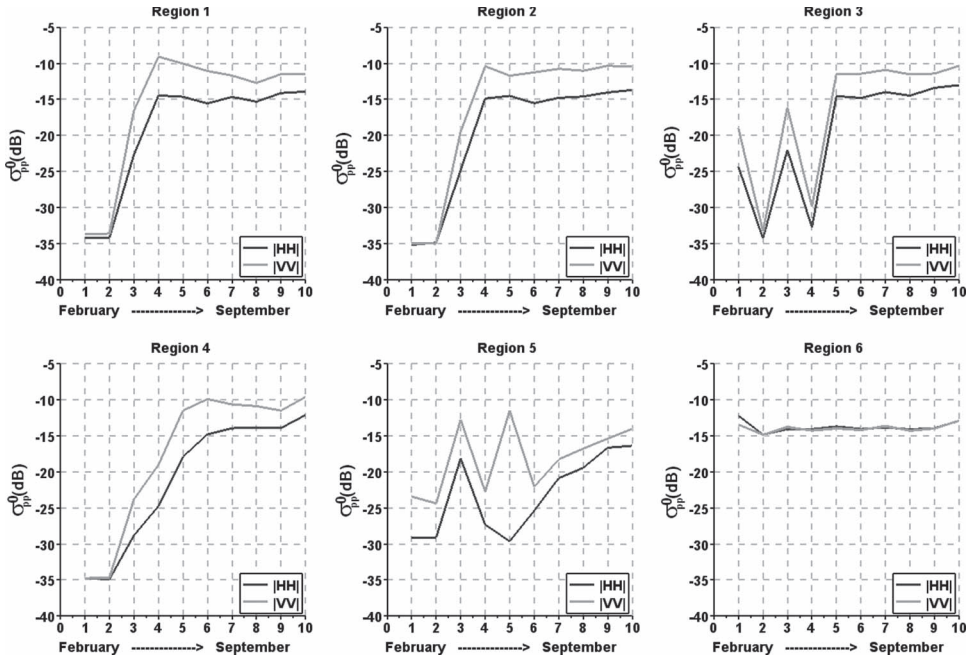

Fig. 6. Temporal variation of the HH and VV backscattered power for the six regions of interest.

least related, if not similar. In addition, the Fresnel coefficients are used in nearly all analytical models proposed in the SAR literature (in particular, the IEM that we shall consider later); hence, starting with the study of their phase behavior makes sense. When an incident planar wave reaches a medium of dielectric constant ε with an incidence angle θ, part of it is transmitted into the medium, and part of it is reflected. The ratio between the reflected and incident waves is expressed by the Fresnel reflection coefficients [2], which depend on the polarization of the incident wave, as follows:

$$R_{\rm hh}=\frac{\cos\theta-\sqrt{\varepsilon-\sin^2\theta}}{\cos\theta+\sqrt{\varepsilon-\sin^2\theta}}\quad R_{\rm vv}=\frac{\sqrt{\varepsilon-\sin^2\theta}-\varepsilon\cos\theta}{\sqrt{\varepsilon-\sin^2\theta}+\varepsilon\cos\theta}. \quad (5)$$

For a pure real value of the dielectric constant ε, the argument of the $R_{\rm hh}$ coefficient is $+180^\circ$ whatever the incidence angle θ. The argument of the $R_{\rm vv}$ coefficient is also $+180^\circ$, for an incidence angle lower than the Brewster incidence angle $\theta_B = \arctan(\sqrt{\varepsilon})$, and becomes 0°, for an incidence angle higher than the Brewster angle. At the Brewster angle, all the incident wave in vertical polarization is transmitted into the medium (the module of the reflection coefficient $R_{\rm vv}$ becomes zero, and its argument changes by 180°). When the dielectric constant of the medium is a complex number, which is the case for saline materials, the Fresnel reflection coefficients are also complex numbers, which arguments are not the same when considering horizontal or vertical polarization.

As a first approximation, we propose to estimate the copolarized phase difference $\Phi_{\rm HHVV}$ as

$$\Phi_{\rm HHVV} = \arg(R_{\rm hh}) - \arg(R_{\rm vv}). \quad (6)$$

In the case of a medium with a pure real dielectric constant, the copolarized phase difference obtained by relationship (6) will then be equal to 0° for an incidence angle lower than the Brewster angle. Fig. 7 shows the copolarized phase difference, computed using (6) for dry salt, of the complex dielectric

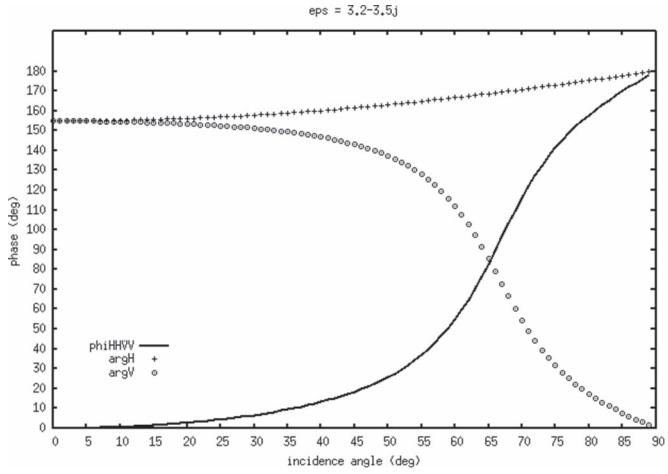

Fig. 7. Argument of Fresnel reflection coefficients $R_{\rm hh}$ (cross) and $R_{\rm vv}$ (circle) with respect to the incidence angle θ for dry salt ($\varepsilon = 3.2 - 3.5$j, $\theta_B = 65.3^\circ$). The copolarized phase difference $\Phi_{\rm HHVV}$ computed using (6) is represented as a plain line.

constant $\varepsilon = 3.2 - 3.5$j at the C-band [15]. The argument of the Fresnel coefficient in horizontal polarization does not change much, with respect to the incidence angle, whereas the argument of the Fresnel reflection coefficient in vertical polarization is dramatically decreasing when approaching the Brewster angle (here, $\theta_B = 65.3^\circ$): at this angle, most of the incident wave in the vertical polarization is transmitted into the medium (the module of the $R_{\rm vv}$ coefficient becomes close to zero, and its argument changes dramatically). The phase difference $\Phi_{\rm HHVV}$ as expressed by (6) is then increasing when the incidence angle θ increases toward the Brewster angle (see plain line in Fig. 7). For the incidence angle of 38.5° of our RADARSAT-2 scenes, we compute a theoretical copolarized phase difference of 12.1° for dry salt using (6). It should be noted that, for low incidence angles ($\theta < 15^\circ$), the arguments of $R_{\rm hh}$ and $R_{\rm vv}$ coefficients are very close, yielding a copolarized phase difference close to 0°.

This approach, which allows to explain the copolarized phase difference only by the complex dielectric constant of saline soils, is quite simple and agrees well with previous observations made over evaporitic surfaces. A more elaborate modeling approach can be developed, using the IEM proposed by Fung *et al.* [9], [10] as a start point. The backscattered wave by an interface can be expressed as the sum of two far-zone backscattered fields: the standard Kirchhoff surface field and the complementary surface field, i.e.,

$$E^s_{\rm pp} = E^k_{\rm pp} + E^c_{\rm pp} \tag{7}$$

where pp represents the polarization state of the incident and backscattered waves. Since we are interested in the copolarized phase only, pp will be either hh or vv. After Fung *et al.* [9], the expression of the Kirchhoff field is

$$E^k_{\rm pp} = CE_0 \int f_{\rm pp} e^{j[(\vec{k}_s - \vec{k}_i)\cdot\vec{r}]} dx\, dy = CE_0 f_{\rm pp} I_k \tag{8}$$

and the expression of the complementary field is

$$\begin{aligned} E^c_{\rm pp} &= \frac{CE_0}{8\pi^2} \int F_{\rm pp} e^{j[u(x-x')+v(y-y')+\vec{k}_s\cdot\vec{r}'-\vec{k}_i\cdot\vec{r}]} \\ &\quad \times dx\, dy\, dx'\, dy'\, du\, dv \\ &= \frac{CE_0}{8\pi^2} F_{\rm pp} I_c \end{aligned} \tag{9}$$

where $C = (-jk/4\pi r)e^{-jk}$, E_0 is the amplitude of the incident electric field, $f_{\rm pp}$ is the Kirchhoff coefficient, and $F_{\rm pp}$ is the complementary coefficient. The far-zone backscattered field can then be written as

$$E^s_{\rm pp} = CE_0 \left(f_{\rm pp} I_k + \frac{F_{\rm pp} I_c}{8\pi^2} \right). \tag{10}$$

The $f_{\rm pp}$ and $F_{\rm pp}$ coefficients can be approximated in forms that only depend on the incidence angle θ of the incident wave and on the dielectric constant ε of the interface: they are then complex quantities if the dielectric constant ε is a complex number. Simplified expressions for the Kirchhoff and complementary field coefficients are given by [10]

$$f_{\rm hh} = \frac{-2R_{\rm hh}}{\cos\theta} \qquad f_{\rm vv} = \frac{2R_{\rm vv}}{\cos\theta} \tag{11}$$

$$F_{\rm hh} = -2\frac{\sin^2\theta}{\cos\theta}\left[4R_{\rm hh} - \left(1 - \frac{1}{\epsilon}\right)(1+R_{\rm hh})^2 \right] \tag{12}$$

$$\begin{aligned} F_{\rm vv} = 2\frac{\sin^2\theta}{\cos\theta}\Bigg[&\left(1 - \frac{\epsilon\cos^2\theta}{\epsilon - \sin^2\theta}\right)(1-R_{\rm vv})^2 \\ &+ \left(1 - \frac{1}{\epsilon}\right)(1+R_{\rm vv})^2 \Bigg]. \end{aligned} \tag{13}$$

With the backscattered field $E^s_{\rm pp}$ being a complex quantity, we can use (10) in order to express the copolarized phase difference $\Phi_{\rm HHVV}$ as

$$\begin{aligned} \Phi_{\rm HHVV} &= \arg\left(E^s_{\rm hh}\right) - \arg\left(E^s_{\rm vv}\right) \\ &= \arg\left(f_{\rm hh} I_k + \frac{F_{\rm hh} I_c}{8\pi^2}\right) - \arg\left(f_{\rm vv} I_k + \frac{F_{\rm vv} I_c}{8\pi^2}\right). \end{aligned} \tag{14}$$

When the scattering interface is very rough, the Kirchhoff field predominates over the complementary field, i.e., $E^k_{\rm pp} \gg E^c_{\rm pp}$, leading to $f_{\rm pp} I_k \gg (F_{\rm pp} I_c / 8\pi^2)$. We can then rewrite the relationship (14) as

$$\Phi_{\rm HHVV} \simeq \arg(f_{\rm hh} I_k) - \arg(f_{\rm vv} I_k) = \arg(f_{\rm hh}) - \arg(f_{\rm vv}). \tag{15}$$

Considering the expressions for the $f_{\rm pp}$ coefficients given by (11), the previous relationship is actually similar to the simple expression proposed in (6). It means that, for very rough surfaces (Kirchhoff approximation case), the copolarized phase difference only depends on the argument of the Fresnel reflection coefficients.

Let us now consider a "medium rough" case, i.e., the Kirchhoff and complementary fields are comparable. In that case, (8) and (9) indicate that $f_{\rm pp} I_k$ and $F_{\rm pp} I_c / 8\pi^2$ should be of the same order. Making the assumption that $f_{\rm pp}$ and $F_{\rm pp}$ coefficients are close, and taking in addition $I_k \simeq (I_c / 8\pi^2)$, allows to simplify relationship (14) into

$$\begin{aligned} \Phi_{\rm HHVV} &\simeq \arg\left[\frac{I_c}{8\pi^2}(f_{\rm hh} + F_{\rm hh})\right] - \arg\left[\frac{I_c}{8\pi^2}(f_{\rm vv} + F_{\rm vv})\right] \\ &= \arg(f_{\rm hh} + F_{\rm hh}) - \arg(f_{\rm vv} + F_{\rm vv}). \end{aligned} \tag{16}$$

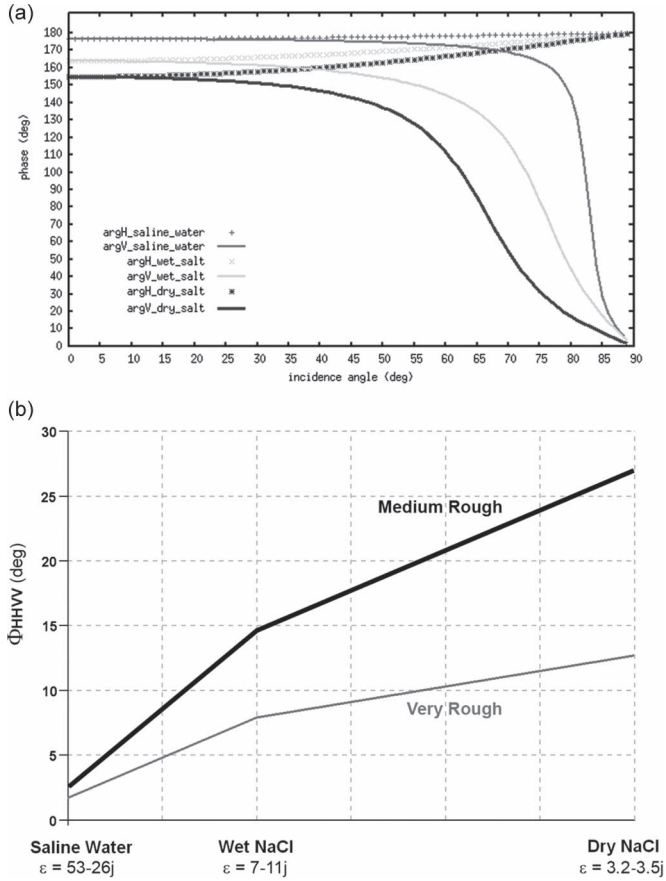

Fig. 8. (a) Argument of Fresnel reflection coefficients for saline water ($\varepsilon = 53 - 26$j, medium gray curves), wet salt ($\varepsilon = 7 - 11$j, light gray curves), and dry salt ($\varepsilon = 3.2 - 3.5$j, dark gray curves) with respect to the incidence angle θ. (b) Modeled copolarized phase difference $\Phi_{\rm HHVV}$ for three types of surfaces, representing different states of the evaporation process for the very rough (gray curve) and medium rough (black curve) case, incidence angle is $\theta = 38.5°$.

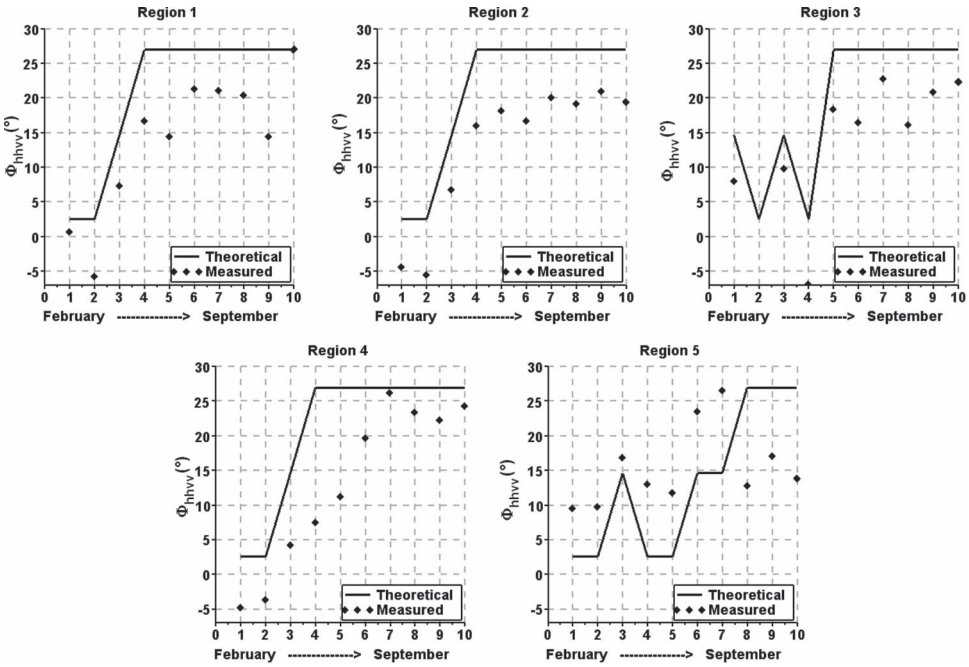

Fig. 9. Observed (dots) and modeled (line) values of the copolarized phase difference Φ_{HHVV} for the five regions of interest located inside the chott El Djerid depression.

Both expressions for the copolarized phase difference given by (15) and (16) only depend on the incidence angle θ and on the dielectric constant ε of the interface. Setting an incidence angle value $\theta = 38.5°$, we then considered three types of surfaces, whose dielectric constants at the C-band were derived in [15], and which are representative of the evaporation process from a smooth liquid surface to a rough dry surface:

— smooth saline water surface with $\varepsilon = 53 - 26\mathrm{j}$ $(\theta_B = 82.6°)$;
— wet crystallized NaCl medium-rough surface with $\varepsilon = 7 - 11\mathrm{j}$ $(\theta_B = 74.5°)$;
— dry crystallized NaCl rough surface with $\varepsilon = 3.2 - 3.5\mathrm{j}$ $(\theta_B = 65.3°)$.

Fig. 8(a) shows the argument of the Fresnel reflection coefficients in horizontal and vertical polarizations for the three types of surfaces. One can notice that, when going from the wettest to the driest case, the Brewster angle θ_B is decreasing from 82.6° to 65.3°: this is consistent with an increase in the copolarized phase difference, as described earlier by (6). Fig. 8(b) shows the evolution of the copolarized phase difference, when going from the wet to the dry case, which is computed using (15) and (16). While the simple expression in (15) does not allow to reproduce a phase difference higher than 12° for dry salt deposits, the "medium roughness" expression in (16) is able to model the increase of Φ_{HHVV} from 0° to more than 28°, as observed on the chott El Djerid as the saline water surfaces evaporate.

Using the previous three representative cases (saline water, wet salt, and dry salt), we then tried to reproduce the observed temporal variations of the copolarized phase difference for the five regions of interest located inside the chott depression. A comparison between observed and computed values of Φ_{HHVV} is presented in Fig. 9: we can fairly well reproduce the variations of Φ_{HHVV} from February to September, i.e., a phase difference change of about 25° between the wet and dry seasons. Of course, we would need to consider more intermediate cases, between the saline water and dry salt extreme cases, in order to better match the observed values, but the simple approach proposed here is already able to reproduce the main trends of the observed phenomena.

V. Conclusion

Using time series of RADARSAT-2 polarimetric acquisitions, we monitored the temporal evolution of the copolarized phase difference over the evaporitic sediments of the chott El Djerid playa. The phase difference at the C-band increases from 0° to close to 25°, when the chott depression evolves from a flooded surface to a dry salt pan. We proposed a simple explanation for this phenomenon, which is based on the argument of Fresnel reflection coefficients when dealing with materials of complex dielectric constant. A more developed theoretical expression for the copolarized phase difference was derived using the IEM approach, which allowed to fairly well reproduce the temporal variations of the phase difference over the chott depression. Among natural surfaces, only the ones containing salt are likely to present a complex dielectric constant: a nonzero value for Φ_{HHVV} is then likely to provide a unique and unambiguous polarimetric signature to detect and monitor saline soils and salt deposits. Our results open new applications for radar polarimetry to monitor the salinization process of agricultural soils and to detect locations in arid environments where groundwater is close to the surface, thus guiding the prospecting for water resources. Future studies will concentrate on field work validation of the proposed model and on the evaluation of the potentials of longer wavelengths (L-band of the Japanese Advanced Land Observing Satellite2 (operated by Japanese Space Agency) SAR; P-band of the Biomass mission of the European Space Agency project).

ACKNOWLEDGMENT

The authors would like to thank the Canadian Space Agency for providing RADARSAT-2 data in the framework of the Science and Operational Applications Research (of Canadian Space Agency)-592 project and three anonymous reviewers for their very useful and relevant comments.

REFERENCES

[1] D. J. Archer and G. Wadge, "Modeling the backscatter response due to salt crust development," *IEEE Trans. Geosci. Remote Sens.*, vol. 39, no. 10, pp. 2307–2310, Oct. 2001.

[2] M. Born and E. Wolf, *Principles of Optics*, 6th corrected. Cambridge, U.K.: Cambridge Univ. Press, 1998.

[3] R. G. Bryant, B. W. Sellwood, A. C. Millington, and N. A. Drake, "Marine-like potash evaporite formation on a continental playa: Case study from the Chott El Djerid, southern Tunisia," *Sedimentary Geol.*, vol. 90, no. 3/4, pp. 269–291, May 1994.

[4] R. G. Bryant, "Application of AVHRR to monitoring a climatically sensitive playa. Case study: Chott El Djerid, southern Tunisia," *Earth Surf. Process. Landforms*, vol. 24, no. 4, pp. 283–302, Apr. 1999.

[5] R. G. Bryant and M. P. Rainey, "Investigation of flood inundation on playas within the zone of Chotts, using a time-series of AVHRR," *Remote Sens. Environ.*, vol. 82, no. 2/3, pp. 360–375, Oct. 2002.

[6] A. Freeman, T. Farr, Ph. Paillou, Y. Lasne, and B. Campbell, "Modeling surface and subsurface scattering from saline soils," presented at the Proc. PolInsar, Frascati, Italy, Jan. 2007.

[7] A. Freeman, Ph. Paillou, Y. Lasne, B. Campbell, K. McDonald, and T. Farr, "Phase differences in longer wavelength polarimetric SAR: Surface or subsurface effects?" presented at the IEEE Int. Geoscience Remote Sensing Symp., Boston, MA, USA, Jul. 2008, Paper MO3.101.3.

[8] P.-L. Frison, Ph. Paillou, N. Sayah, E. Pottier, and J.-P. Rudant, "Spatio-temporal monitoring of evaporitic processes using C-band radar remote sensing data: Example over the chott el Djerid, Tunisia," *Can. J. Remote Sens.*, vol. 39, no. 2, pp. 127–137, 2013.

[9] A. K. Fung, Z. Li, and K. S. Chen, "Backscattering from a randomly rough dielectric surface," *IEEE Trans. Geosci. Remote Sens.*, vol. 30, no. 2, pp. 356–369, Mar. 1992.

[10] A. K. Fung, *Microwave Scattering and Emission Models and Their Applications*. Norwood, MA, USA: Artech House, 1994.

[11] S. Kamel, L. Dassi, K. Zouari, and B. Abidi, "Geochemical and isotopic investigation of the aquifer system in the Djerid-Nefzaoua basin, southern Tunisia," *Environ. Geol.*, vol. 49, no. 1, pp. 159–170, Nov. 2005.

[12] Y. Lasne, Ph. Paillou, Th. August-Bernex, G. Ruffié, and G. Grandjean, "A phase signature for detecting subsurface wet structures using polarimetric L-band SAR data," *IEEE Trans. Geosci. Remote Sens.*, vol. 42, no. 8, pp. 1683–1694, Aug. 2004.

[13] Y. Lasne, Ph. Paillou, G. Ruffié, and M. Crapeau, "Effect of multiple scattering on the phase signature of wet subsurface structures: Applications to polarimetric L and C-band SAR," *IEEE Trans. Geosci. Remote Sens.*, vol. 43, no. 8, pp. 1716–1726, Aug. 2005.

[14] Y. Lasne, Ph. Paillou, G. Ruffié, C. Serradilla, J.-M. Malézieux, A. Freeman, T. Farr, and K. McDonald, "Effect of salinity on the dielectric properties of geological materials: Implication on soil moisture detection by means of remote sensing," *IEEE Trans. Geosci. Remote Sens.*, vol. 46, no. 6, pp. 1674–1688, Jun. 2008.

[15] Y. Lasne, Ph. Paillou, A. Freeman, T. Farr, K. McDonald, G. Ruffié, J.-M. Malézieux, and B. Chapman, "Study of hyper-saline deposits and analysis of their signature in airborne and spaceborne SAR data: Example of Death Valley, California," *IEEE Trans. Geosci. Remote Sens.*, vol. 47, no. 8, pp. 2581–2598, Aug. 2009.

[16] J.-S. Lee and E. Pottier, *Polarimetric Radar Imaging: From Basics to Applications*. Boca Raton, FL, USA: CRC Press, 2009.

[17] "RADARSAT-2 product description," MDA, Richmond, BC, Canada, RN-SP-52-1238, Nov. 2009, 1–6.

[18] C. R. Roberts and C. W. Mitchell, "Spring mounds in southern Tunisia," in *Desert Sediments: Ancient and Modern*, L. Frostick and I. Reid, Eds. London, U.K.: Geol. Soc., 1987, pp. 321–334.

[19] K. Sarabandi, "Derivation of phase statistics from the Mueller matrix," *Radio Sci.*, vol. 27, no. 5, pp. 553–560, Sep./Oct. 1992.

[20] Y. Shao, Q. Hu, H. Guo, Y. Lu, Q. Dong, and C. Han, "Effect of dielectric properties of moist salinized soils on backscattering coefficients extracted from RADARSAT image," *IEEE Trans. Geosci. Remote Sens.*, vol. 41, no. 8, pp. 1879–1887, Aug. 2003.

[21] K. Sreenivas, L. Venkataratnam, and P. V. Narasimha Rao, "Dielectric properties of salt-affected soils," *Int. J. Remote Sens.*, vol. 16, no. 4, pp. 641–649, Mar. 1995.

[22] C. S. Swezey, "Structural controls on Quaternary depocentres within the Chotts Trough region of southern Tunisia," *J. African Earth Sci.*, vol. 22, no. 3, pp. 335–347, Apr. 1996.

[23] G. R. Taylor, A. H. Mah, F. A. Kruse, K. S. Kierein-Young, R. D. Hewson, and B. A. Bennet, "Characterization of saline soils using airborne radar imagery," *Remote Sens. Environ.*, vol. 57, no. 3, pp. 127–142, Sep. 1996.

[24] F. T. Ulaby, R. K. Moore, and A. K. Fung, *Microwave Remote Sensing: Active and Passive*. Norwood, MA, USA: Artech House, 1982.

[25] G. Wadge, D. J. Archer, and A. C. Millington, "Monitoring playa sedimentation using sequential radar images," *Terra Res.*, vol. 6, no. 4, pp. 391–396, Jul. 1994.

[26] G. Wadge and D. J. Archer, "Evaporation of groundwater from arid playas measured by C-band SAR," *IEEE Trans. Geosci. Remote Sens.*, vol. 41, no. 7, pp. 1641–1650, Jul. 2003.

Philippe Paillou received the Engineer Diploma from the Ecole Nationale Supérieure de Physique de Strasbourg, Strasbourg, France, in 1989 and the Ph.D. degree in image processing from the University of Strasbourg, Strasbourg, France, in 1992.

Since 2004, he has been a Full Professor with the University of Bordeaux, UMR 5804 (LAB), Floirac, France. He is involved in several orbital radar missions (Advanced Land Observing Satellite / Phased Array type L-band Synthetic Aperture Radar (operated by Japanese Space Agency), RADAR instrument onboard the CASSINI Spacecraft to Saturn (operated by NASA), and Biomass mission of the European Space Agency), with the aim to study arid regions on Earth and planetary surfaces. He served as a Scientific Advisor for the Earth Observation Division, French Space Agency (CNES), Paris, France; the Mission Science Division, European Space Agency, Noordwijk, The Netherlands; and the Planetary Science Division, NASA. He published more than 50 papers in international journals and presented more than 200 communications in international conferences. His most significant research results are the discovery of impact craters in Libya and Egypt, the discovery of a major paleo-river in Libya, and the participation to the discovery of methane lakes on Titan.

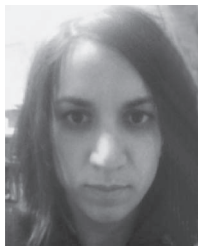

Sarah Sufyar received the Engineer Diploma in electrical engineering, specialized in wireless systems, and the M.Sc. degree in microelectronics from the Ecole Nationale Supérieure d'Electronique, Informatique et Radiocommunication de Bordeaux, Talence, France, both in 2008 and the Ph.D. degree in antenna and radio frequencies from the University of Grenoble, Grenoble, France, in 2011.

She is currently a Postdoctoral Fellow with the Laboratoire de l'Intégration du Matériau au Système (IMS), Pessac, France, in the field of wave propagation theory, antennas, and microwave remote sensing. She is also with the University of Bordeaux, UMR 5804 (LAB), Floirac, France.

Anthony Freeman received the B.S. degree in mathematics and the Ph.D. degree in astrophysics from the University of Manchester Institute of Science and Technology, Manchester, U.K.

He is the Earth Science Manager of the Earth System Science Formulation Office, Jet Propulsion Laboratory, Pasadena, CA, USA. He has over 20 years experience as a technical manager, researcher, system designer and engineer, lecturer, project leader, and task leader. He was the Instrument Manager for the LightSAR Radar Program. His responsibilities included the design and technology development of a lightweight, capable polarimetric, and multimode spaceborne synthetic aperture radar for science and commercial use. He is the holder of two patents.

Dr. Freeman was a recipient of the NASA Exceptional Service Medal for calibration of SIR-C mission data and numerous NASA new technology awards.